Universality and unconventional enhancement of flux-flow resistivity in $Ba(Fe_{1-x}Co_x)_2As_2$

X. Y. Huang,[1] D. J. Haney,[1] Y. P. Singh,[1,*] T. Hu,[1,2] H. Xiao,[1,3] Hai-Hu Wen,[4] M. Dzero,[1] and C. C. Almasan[1]

[1]*Department of Physics, Kent State University, Kent, Ohio, 44242, USA*

[2]*Shanghai Institute of Microsystem and Information Technology, Shanghai 200050, China*

[3]*Center for High Pressure Science and Technology Advanced Research, Beijing 100094, China*

[4]*Nanjing University, Nanjing 210093, China*

(Received 6 December 2016; revised manuscript received 10 March 2017; published 22 May 2017)

Measurements of the current-voltage characteristics (I-V) were performed on $Ba(Fe_{1-x}Co_x)_2As_2$ single crystals with doping level $0.044 \leqslant x \leqslant 0.100$. An unconventional increase in the flux-flow resistivity ρ_{ff} with decreasing magnetic field H was observed across this doping range. Such an abnormal field dependence of ρ_{ff} is in contrast with the linear $\rho_{ff}(H)$ of conventional type-II superconductors, but similar to the behavior recently observed in the heavy-fermion superconductor $CeCoIn_5$. A significantly enhanced ρ_{ff} was found for the $x = 0.06$ single crystals, implying a strong single-particle energy dissipation around the vortex cores. At different temperatures and fields and for a given doping concentration, the normalized ρ_{ff} scales with normalized field and temperature. The doping level dependence of the scaling parameters strongly suggests that the abnormal upturn in ρ_{ff} is likely related to the enhancement of spin fluctuations around the vortex cores of the samples with $x \approx 0.06$.

DOI: 10.1103/PhysRevB.95.184513

I. INTRODUCTION

The cobalt-doped superconducting (SC) iron-arsenide material $Ba(Fe_{1-x}Co_x)_2As_2$ has been widely studied due to the presence of a magnetic phase transition above the zero-field superconducting critical temperature T_{c0} [1–3] and the microscopic coexistence of magnetic and superconducting phases under the superconducting dome [1]. The latter finding also provides the motivation to investigate whether these phases may be governed by the system's proximity to a putative quantum critical point (QCP) [4–6]. Recently, the coexistence of superconductivity and spin-density wave (SDW) phases has been further confirmed by NMR measurements, in which a spin glass phase is revealed between $x = 0.06$ and 0.071 [7]. Intriguingly, within the framework of the multiband theory of superconductivity, the doping-induced disorder seems to play a major role in suppressing the magnetic order while giving rise to emergent superconducting order since the superconductivity remains immune to the intraband disorder-induced scattering processes while SDW order does not [8].

Flux-flow resistivity ρ_{ff} measurements offer a crucial insight into competing interactions of a superconducting system since the energy dissipation due to the motion of the flux vortices in the Ohmic regime is sensitive to the fluctuations of the corresponding order parameters [9], either of magnetic or some other origin. In these measurements one traces the evolution of ρ_{ff} (the slopes in the current-voltage I-V characteristics) with magnetic field and temperature and, in principle, extracts information about the band structure [10] as well as relevance of various dissipation mechanisms to the transport properties of flux vortices. The idea behind the experiment [9] originates from the following observation: the dissipation in the form of flux-flow resistivity is strongly affected by the magnetic fluctuations around the vortex cores of an unconventional superconducting system in the proximity to a magnetic instability.

In this paper we use our improved I-V measurement method to probe the physics related to the coexistence of magnetic and superconducting phases in $Ba(Fe_{1-x}Co_x)_2As_2$ (see Fig. 1) by exploring the vortex behavior that could be affected by the secondary (in relation to superconductivity) phases in the mixed state. We find that an abnormal flux-flow resistivity as a function of magnetic field appears over a wide range of doping. Intriguingly, we find that the $x = 0.06$ single crystal shows the largest upturn caused by the strongest dissipation among the five doping levels we have studied. We naturally interpret this observation as an indication that the secondary phase has the strongest effect for the $x \approx 0.06$ single crystals. In addition, we reveal a universal scaling behavior of the flux-flow resistivity data obtained at different magnetic fields and temperatures for different Co doping for this $Ba(Fe_{1-x}Co_x)_2As_2$ system (see below). We investigate how the parameters which enter this scaling function change with doping. While the scaling form of the flux-flow resistivity with magnetic field is universal for the whole doping range studied, the variation of the other two scaling parameters allows us to identify three regimes with distinctive dependence of the flux-flow resistivity on doping and temperature. All these results point to a strong magnetic field H and temperature T dependence of the viscosity coefficient η as a result of the system's proximity to a magnetic instability.

II. EXPERIMENTAL DETAILS

Single crystals of $Ba(Fe_{1-x}Co_x)_2As_2$ were grown using the FeAs self-flux method [3,11]. The actual Co-doping level x of each single crystal was determined by comparing its zero-field superconducting transition temperature T_{c0} value to well-established T_{c0}-x phase diagrams for this system [3,11,12]. As shown in Fig. 1, the doping levels of the single crystals discussed in this paper are $x = 0.044$, 0.056, 0.060, 0.072, and 0.100, which cover the underdoped, optimally

*Present address: Department of Mechanical Engineering, The University of Akron, Akron, Ohio 44325, USA.

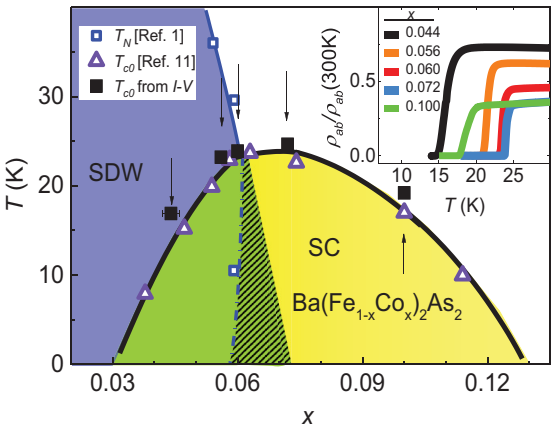

FIG. 1. Sketch of the temperature-doping T-x phase diagram for $Ba(Fe_{1-x}Co_x)_2As_2$. The phases depicted on this phase diagram are: SDW (purple region), coexistence of SC and SDW phases [1] (green region), spin glass phase [7] (hatched green region), and pure SC phase (yellow region). The arrows mark the five doping levels discussed in this paper. Inset: In-plane resistivity normalized to its value at 300 K, $\rho/\rho(300\ \mathrm{K})$, measured in zero field and for five doping levels.

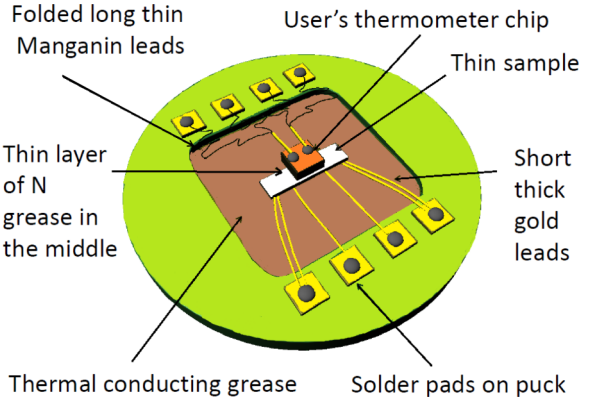

FIG. 2. Schematic drawing of the current-voltage I-V measurement configuration that takes care of Joule heating caused by the large applied current.

doped, and overdoped regimes. The temperature and magnetic field dependence of the electrical resistivity ρ was measured on thin single crystals using the standard four-probe method with current flowing in the ab plane and H applied along the crystallographic c axis. The inset to Fig. 1 shows that all the single crystals studied here have sharp superconducting transitions.

We also performed I-V measurements as a function of T and H. Due to strong vortex pinning present in the mixed state of these superconductors, we had to apply a large current ($I \leqslant 160$ mA). In order to maximize the current density (desirable for the effective depinning of the flux vortices), the cross-section area A of the single crystals was reduced down to 0.17×0.04 mm^2; indeed, for a given heating power per unit length l, a maximum current density j is accomplished for an achievable minimum cross-section area A since $l \equiv (I^2R)/L = (j^2A^2)(\rho L/A)/L = j^2\rho A$.

To minimize the Joule heating of the gold current leads and also to increase the heat transport from the single crystal to the thermal bath, multiple short thick gold current leads were used for the two current terminals (see Fig. 2) since for a given applied current, the dissipated power $P = I^2R = I^2\rho L/A$. Also, we used Sn, instead of silver paste, in order to decrease the contact resistance between the single crystal and the current leads down to less than 10 $\mu\Omega$ [13].

In order to increase the temperature stability and to be able to apply large currents, we have also improved our measuring protocol and apparatus. We added an additional thermometer, mounted on the top of the sample using N-type grease, which we used to control and measure the temperature of the sample, and we used long folded manganin wires as terminal leads of this additional thermometer in order to decrease the heat transport between the thermometer and puck, since manganin has poor thermal conduction. After the temperature was deemed stable, a 60 s wait time (with the persistent current flowing through the single crystal) was included into the measurement sequence and only then the I-V data were collected. Finally, we used a combination of Linear Research ac resistance bridge LR700 with extended current limit and Physical Property Measurement System (PPMS) to carry out the I-V measurements. Due to the high current limit imposed by our experimental conditions ($I \approx 160$ mA) and the fact that vortex pinning increases with decreasing temperature, all the I-V measurements were done at temperatures $0.87\ T_{c0} \leqslant T \leqslant 0.98\ T_{c0}$, i.e., about 2 K below the H-T phase boundary. Using all the improvements in our experimental technique mentioned above, we were able to reduce the temperature instability due to Joule heating to less than 0.1 K.

III. RESULTS

A. Current-voltage characteristics

The electrical resistivity in the mixed state of type-II superconductors in the presence of an applied magnetic field is mainly governed by the motion of Abrikosov vortices [14]. When the Lorentz force is larger than the pinning force, the flux vortices are driven into a viscous-flow state. The flux-flow resistivity ρ_{ff} is defined as $\rho_{ff} \equiv kdV/dI$, where dV/dI is the slope of the linear region of the I-V curves and k is the geometric factor. The intercept obtained by extrapolating the linear $V(I)$ region to zero voltage gives the value of the critical current I_c. The flux flow is solely determined by the bulk properties of the material. Therefore, the I-V measurement under the superconducting dome is a probe that takes advantage of the fact that an external magnetic field induces vortices in type-II superconductors that form islands of dissipative matter embedded in the nondissipative superconductor and allows one to measure the dissipation of these flux vortices. Consequently, the application of this technique makes it possible to probe the interaction between superconducting and normal regions of a sample at the length scale determined by the vortex size, as flux vortices move through the superconductor.

Figures 3(a), 4(a), and 4(b) show I-V data measured in the mixed state of $Ba(Fe_{1-x}Co_x)_2As_2$ with $x = 0.060$, 0.044, and 0.100, respectively, at different field values. These I-V

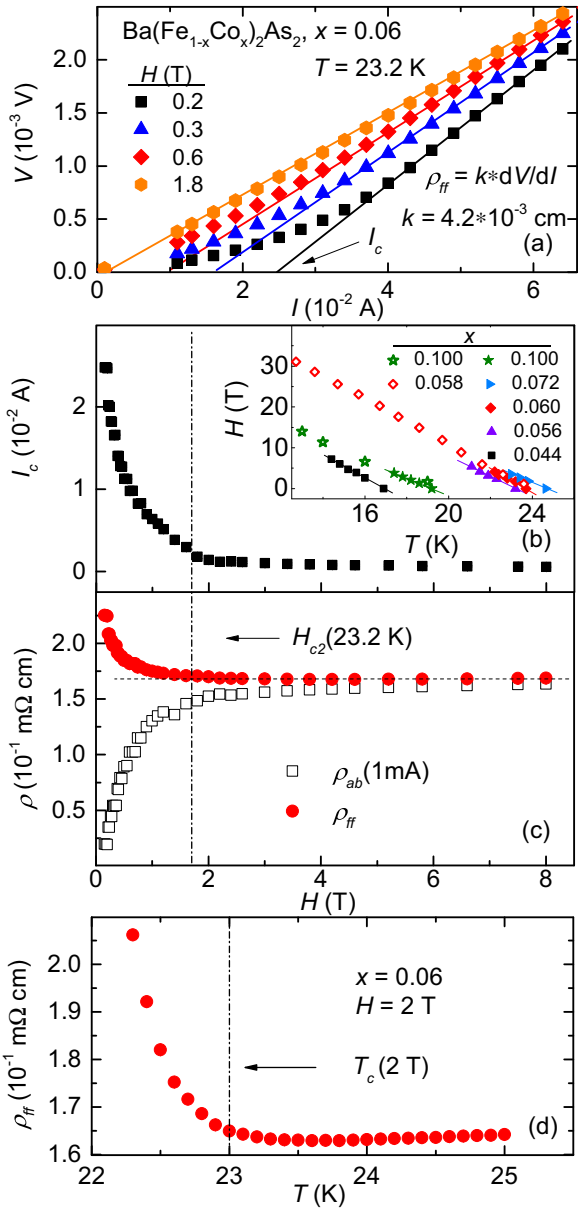

FIG. 3. (a) Current-voltage I-V curves measured in the mixed state of $Ba(Fe_{1-x}Co_x)_2As_2$ ($x = 0.060$) single crystal at a temperature T of 23.2 K and different magnetic field H values. (b) Plot of the critical current I_c vs H. Inset to (b): H-T phase diagram obtained from this work (filled symbols) and from [11] (open symbols). (c) H dependence of the flux-flow resistivity ρ_{ff} (filled circles) and the resistivity ρ_{ab} measured with a constant current of 1 mA applied parallel with the ab plane of the single crystal (open squares). (d) ρ_{ff} vs T measured at 2 T on the $x = 0.060$ single crystal.

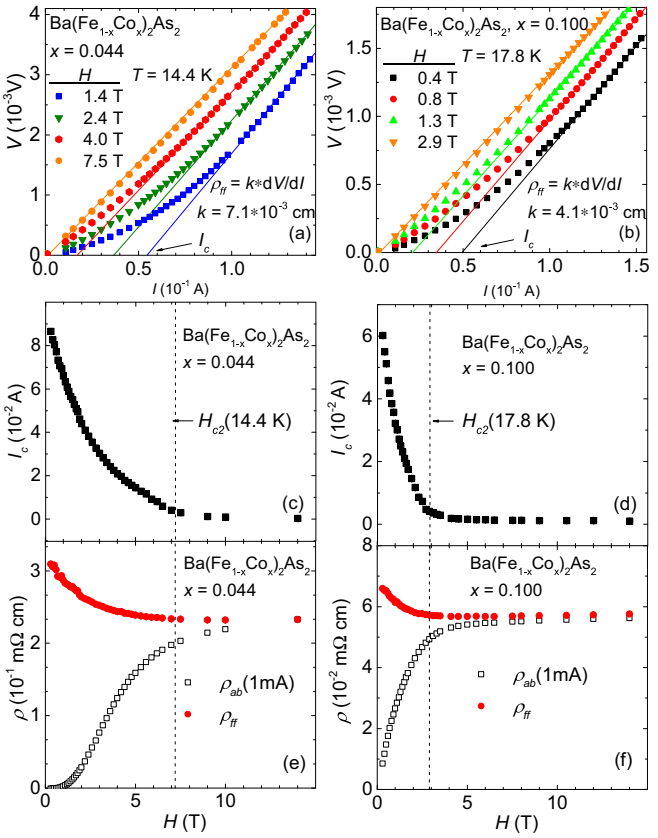

FIG. 4. Current-voltage I-V curves measured at different magnetic field H values in the mixed state of $Ba(Fe_{1-x}Co_x)_2As_2$ with (a) $x = 0.044$ at a temperature T of 14.4 K and (b) $x = 0.100$ at $T = 17.8$ K. Plots of the critical current I_c vs H for (c) $x = 0.044$ and (d) $x = 0.100$. (c) H dependence of the flux-flow resistivity ρ_{ff} (filled circles) and the resistivity ρ_{ab} measured with a constant current of 1 mA applied parallel with the ab plane of the single crystals (open squares) for the (e) the $x = 0.044$ and (f) $x = 0.100$ samples.

characteristics are typical for all the samples studied. The lines show the slopes of the Ohmic regime measured for different H values, which allow us to determine $\rho_{ff}(H)$. Notice that the linear region (Ohmic regime) becomes wider with increasing H and that it extends over the whole current range (the I-V characteristics are straight lines passing through origin) at H values equal to or larger than the upper critical field $H_{c2}(T)$, reflecting the Ohmic behavior of the sample in the normal state. We define the upper critical field H_{c2} corresponding to the measured temperature as the field value for which the I-V lines pass through the origin.

Figures 3(b), 4(c), and 4(d) are plots of $I_c(H)$ extracted from the I-V data of Figs. 3(a), 4(a), and 4(b), respectively, as discussed above. Notice that the $I_c(H)$ curves show a noticeable and systematic increase with decreasing field below a certain magnetic field value, marked by the vertical dotted lines. We define this field value below which the critical current increases as the upper critical field H_{c2} corresponding to this temperature. We note that this definition of H_{c2} is consistent with the definition given based on the I-V curves at the end of the previous paragraph. For example, both Figs. 3(a) and 3(b) give $H_{c2} = 1.8$ T at $T = 23.2$ K.

The inset to Fig. 3(b) shows the H-T phase diagram generated as just discussed for the Co doping studied here (filled symbols) and from published resistivity data (open symbols) in which $H_{c2}(T)$ is defined as the onset in the SC transition in $\rho(H)$ curves measured at multiple temperatures [11]. Notice the good agreement between our results and published results, supporting our definitions of $H_{c2}(T)$ presented above.

Figures 3(c), 4(e), and 4(f) show the field dependence of ρ_{ff} (red filled circles) extracted from the I-V curves shown

in Figs. 3(a), 4(a), and 4(b), respectively, along with the resistivity ρ_{ab} measured using a low constant current of 1 mA applied in the ab plane of the crystal (open squares). The difference between the $\rho_{\rm ff}$ and ρ_{ab} curves at low H values (in the mixed state) is a result of the fact that the red circles data give the flux-flow dissipation of the vortices in the Ohmic regime where pinning is negligible, while the data shown as squares give the dissipation of the vortices in the non-Ohmic regime where pinning dominates. The two curves do not overlap just above $H_{c2}(T)$ most likely since ρ_{ab} displays superconducting fluctuations while in $\rho_{\rm ff}$ these fluctuations are suppressed due to larger currents. We note that this result is in contrast with the one obtained by some of us on $CeCoIn_5$ [9], for which $\rho_{\rm ff}$ and ρ_{ab} overlap just above H_{c2}. A likely reason for the different behavior in these two systems is that $Ba(Fe_{1-x}Co_x)_2As_2$ is much more anisotropic than $CeCoIn_5$, hence the SC fluctuations are stronger in the former system. As expected, in the normal state at higher field values both sets of data corresponding to the two measurements overlap within around 4%, and both $\rho_{\rm ff}$ and ρ_{ab} show a weak field dependence, reflecting the weak magnetoresistance of this sample.

Type-II superconductors display a well known linear relationship between $\rho_{\rm ff}$ and H at low H values, with $\rho_{\rm ff}/\rho_{\rm n} \propto H/H_{c2}$, where $\rho_n \equiv \rho_{\rm ff}(H_{c2})$ [15], and its saturation near H_{c2} [16–18]. However, the upturn of $\rho_{\rm ff}$ vs H revealed by the data of Figs. 3(c), 4(e), and 4(f) in the mixed state is in contrast with this well known behavior. Since the dissipation of the vortices is dominated by the dissipation of the quasiparticle in the vortex cores at least for $T \sim T_c$, the upturn in $\rho_{\rm ff}$ in the mixed state reflects the increase in the scattering of the quasiparticles in the vortex cores with decreasing applied magnetic field. Hence, the dissipation of the vortices reveals the dominant scattering mechanism of the underlying normal state.

Figure 3(d) shows the temperature dependence of $\rho_{\rm ff}$ extracted from the I-V curves measured at a constant field of 2 T for the $x = 0.060$ single crystal. Notice the sharp increase of $\rho_{\rm ff}$ with decreasing T just below $T_c \approx 23$ K for this value of the applied magnetic field. This behavior is typical for all the samples studied. We note that this nonmetallic vortex dissipation displayed in this figure is in sharp contrast with the metallic dissipation in the normal state. One would expect the scattering of the quasiparticles of the vortex cores and normal state to be very similar to each other near T_c. However, possible deviations from this behavior could occur due to the presence of several competing interactions, as discussed below.

It is well known that the scattering of quasiparticles is enhanced by critical spin fluctuations present close to a magnetic transition. For example, enhanced electrical resistivity due to magnetic spin fluctuations has being reported just above the antiferromagnetic phase transition in the normal state of $CeCo(In_{1-x}Cd_x)_5$ with $x = 0.0075$ [19]. In addition, our magnetoresistivity $MR \equiv \rho(H)/\rho(14\ \text{T}) - 1$ data of the underdoped $Ba(Fe_{1-x}Co_x)_2As_2$ ($x = 0.044$), with a Néel temperature $T_N = 66.3$ K [20] larger than $T_{c0} = 16.6$ K, show as T decreases first a sudden change in slope followed by a peak [Fig. 5(a)]. We identify the structural and magnetic phase transitions as $T_s = 76.6$ K and $T_N = 66.3$ K, respectively, corresponding to these two features in the MR curve, as indicated by the arrows on the figure. These transition temperatures agree with published data of

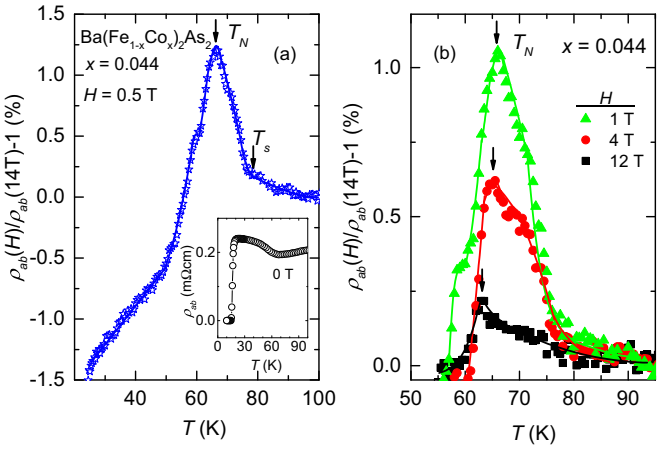

FIG. 5. (a) Temperature T dependent magnetoresistivity MR $\equiv \rho_{ab}(H)/\rho_{ab}(14\ \text{T}) - 1$ curve of the $x = 0.044$ single crystal measured in a magnetic field of 0.5 T and with a current of 1 mA. Inset: ρ_{ab} vs T measured in zero magnetic field. (b) T dependent MR curve for 1, 4, and 12 T.

heat capacity, susceptibility, resistivity, Hall-coefficient, and neutron diffraction measurements on the same doping [1,3,11]. The maximum MR at T_N reflects the maximum quasiparticle scattering due to critical magnetic fluctuations present near T_N [9]. Hence, quasiparticle scattering identifies the presence of critical magnetic fluctuations for systems that are close to a magnetic instability, in this case SDW.

Typical MR data in applied magnetic fields of 1, 4, and 12 T are shown in Fig. 5(b). The position of the maximum in MR shifts to lower temperatures with increasing H, confirming that, indeed, the position of the maximum in MR represents T_N. We note that in plotting MR, we effectively subtracted the background scattering present in a magnetic field of 14 T (at least for $T \geqslant 60$ K) since $T_N < 60$ K for this H value. As a result, we are able to extract the quasiparticle scattering due to spin fluctuations in the vicinity of the SDW order from the total quasiparticle scattering—information unrevealed by the direct measurement of $\rho(T)$ [inset to Fig. 5(a)].

Based on the above discussion, we are led to interpret the observed upturn in $\rho_{\rm ff}(T)$ with decreasing T [Figs. 3(c), 4(e), and 4(f)] as being due to critical antiferromagnetic fluctuations in the vicinity of the boundary separating spin-density-wave and paramagnetic phases. Also, since these magnetic fluctuations are suppressed by a magnetic field, $\rho_{\rm ff}$ is strongly suppressed, as expected, with increasing H [see Figs. 3(c), 4(e), and 4(f)]. The fact that $\rho_{\rm ff}$ starts increasing just below the SC boundary [Figs. 3(c), 3(d), 4(e), and 4(f)] suggests that the dynamic magnetic fluctuations emerge at the SC phase boundary.

We note that the well-known positive slope in $\rho_{\rm ff}(H)$ was observed in some iron-based superconductors like LiFeAs [21], $NaFe_{0.97}Co_{0.03}As$ [22], $BaFe_2(As_{0.55}P_{0.45})_2$ [23], and $FeSe_{0.4}Te_{0.6}$ [24] using a microwave technique. Nevertheless, all these flux-flow studies are done at low temperatures, while our I-V measurements are limited to high temperatures, a few degrees below T_{c0}. Therefore, the difference between the published $\rho_{\rm ff}(H)$ dependence (measured at low temperatures) and the present data (measured at temperatures close to

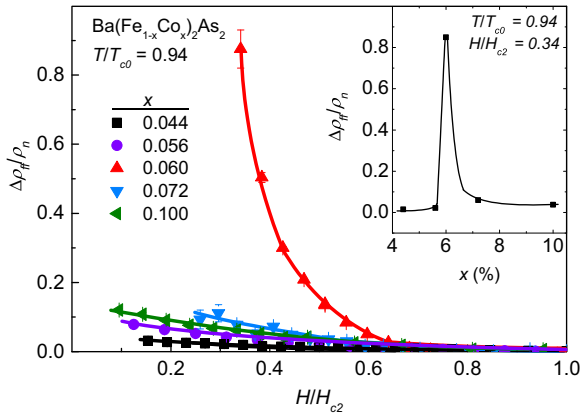

FIG. 6. Normalized flux-flow resistivity $\Delta\rho_{\rm ff}/\rho_{\rm n} \equiv \rho_{\rm ff}/\rho_{\rm n} - 1$ as a function of reduced magnetic field H/H_{c2} measured at the same reduced temperature $T/T_c = 0.94$ for all Co doping values x. Inset: $\Delta\rho_{\rm ff}/\rho_n$ vs x measured at $T/T_c = 0.94$ and $H/H_{c2} = 0.34$ for all the single crystals studied.

T_{c0}) reflects the difference in the scattering mechanism of the quasiparticles in the vortex cores in these two different temperature regimes. One such difference could be that the low T published data are not affected by critical spin fluctuations.

B. Doping dependence of flux-flow resistivity

In Fig. 6 we plot the normalized flux-flow resistivity $\Delta\rho_{\rm ff}/\rho_{\rm n} \equiv \rho_{\rm ff}/\rho_{\rm n} - 1$ as a function of reduced field H/H_{c2} measured at the same reduced temperature $T/T_{c0} = 0.94$ for all doping levels. Notice that $\Delta\rho_{\rm ff}/\rho_{\rm n}$ displays a weak field dependence and a weak change in its value as the doping level increases from $x = 0.044$ (black squares) to $x = 0.056$ (purple circles). However, $\Delta\rho_{\rm ff}/\rho_{\rm n}$ reveals a huge upturn for the $x = 0.060$ single crystal (red triangles), a doping level around optimal doping (see Fig. 1). With further increasing the doping level to the overdoped regime, the upturn decreases to values as low as the ones found in the $x = 0.044$ single crystals.

The fact that the strongest upturn in $\Delta\rho_{\rm ff}/\rho_{\rm n}$ happens at or around optimal doping while it remains rather weak in the underdoped and overdoped regimes indicates a significant increase in the scattering of the quasiparticles around the vortex cores for the $x \approx 0.060$ single crystals. This, in turn, suggests that the critical spin fluctuations are the strongest for the optimally doped Co single crystal, providing a leading contribution to the energy dissipation of the moving flux vortices; hence, it further suggests that the $x = 0.060$ Co doping is right at the phase boundary between a magnetically ordered state (SDW) and a spin disordered state (paramagnetic phase). Indeed, this particular Co doping is the closest, among the doping studied here, to the doping where the SDW phase boundary enters under the SC dome (see Fig. 1). In the underdoped regime of the $Ba(Fe_{1-x}Co_x)_2As_2$ system, the SDW order state coexists with the SC state. Thus, the spin fluctuations around vortex cores should be considerably suppressed, which is consistent with the weak upturn observed in $x = 0.044$ and 0.056. The weak upturn in $\Delta\rho_{\rm ff}$ with decreasing H in the overdoped regime could be a result of the fact that these samples are further away from the SDW phase boundary.

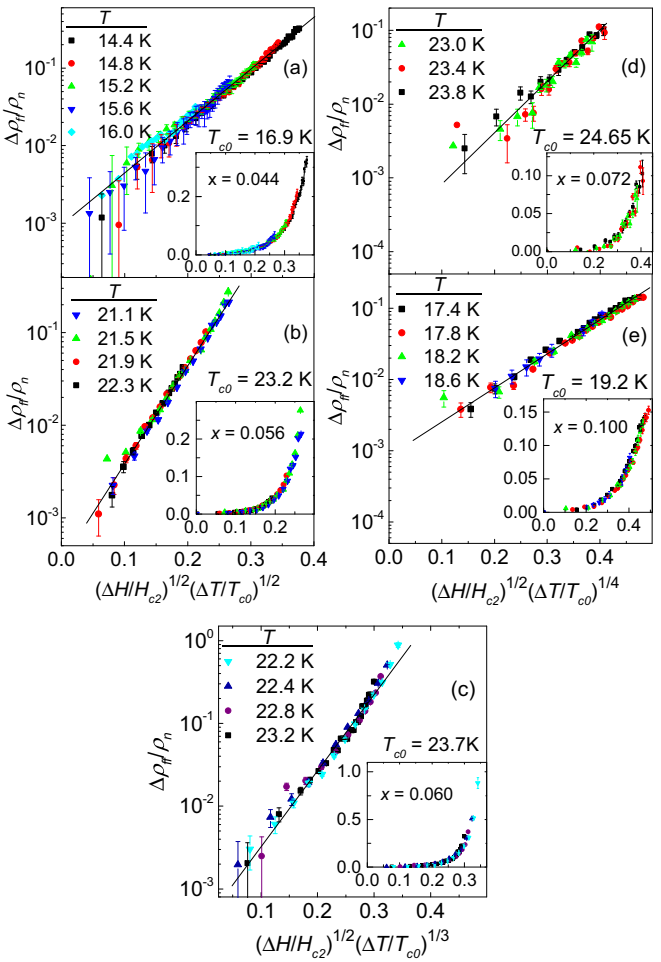

FIG. 7. Semi-log plots of the normalized free-flux-flow resistivity $\Delta\rho_{\rm ff}/\rho_{\rm n}$ vs reduced field and temperature $(\Delta H/H_{c2})^m(\Delta T/T_{c0})^n$ for all five doping levels of $Ba(Fe_{1-x}Co_x)_2As_2$ studied. The straight lines are guides to the eye. Inset: Linear plots of the same data.

C. Scaling behavior

A careful analysis of all the I-V data obtained in different applied magnetic fields, temperatures, and for different Co doping for the $Ba(Fe_{1-x}Co_x)_2As_2$ system reveals a universal scaling behavior between normalized flux-flow resistivity $\Delta\rho_{\rm ff}/\rho_{\rm n}$ and reduced field $\Delta H/H_{c2}$ and temperature $\Delta T/T_{c0}$. Figures 7(a) through 7(e) are semi-log plots of $\Delta\rho_{\rm ff}/\rho_{\rm n}$ as a function of $(\Delta H/H_{c2})^m(\Delta T/T_{c0})^n$ for the five doping levels studied here, while their insets are plots of the same data on a linear scale. Indeed, all these plots show that all the $\Delta\rho_{\rm ff}$ data for the same doping obtained at different fields and temperatures scale for certain values of the scaling parameters m and n, while the linear correlation on the semi-log plot between $\Delta\rho_{\rm ff}$ and $(\Delta H/H_{c2})^m(\Delta T/T_{c0})^n$ reveals an exponential functional dependence. Hence, all the data follow the functional form:

$$\log_{10}(C\,\Delta\rho_{\rm ff}/\rho_{\rm n}) = A(\Delta H/H_{c2})^m(\Delta T/T_{c0})^n, \qquad (1)$$

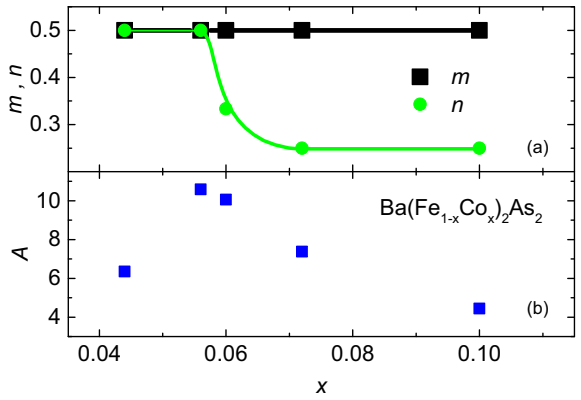

FIG. 8. Doping dependence of the scaling parameters m and n (top panel), and A (bottom panel).

where C is a constant, $\Delta\rho_{\rm ff} \equiv \rho_{\rm ff} - \rho_{\rm n}$, $\Delta H \equiv H_{c2} - H$, and $\Delta T \equiv T_{c0} - T$, while $A(x)$, $m(x)$, and $n(x)$ are mutually independent parameters that only depend on the doping level x. The H_{c2} and T_{c0} values used for the different doping levels were obtained as explained in the discussion related to Fig. 3(b), 4(c), and 4(d) and are shown in the H-T phase diagram of the inset to Fig. 3(b).

The scaling parameters m, n, and A are plotted as a function of the doping x in Figs. 8(a) and 8(b). These figures show that the field dependence of the flux-flow resistivity is the same, $m = 0.5$, across the whole doping range, while the temperature exponent n displays a steplike dependence on x with $n = 1/2$, $1/3$, and $1/4$ for the underdoped, optimally doped, and overdoped range, respectively [see Fig. 8(a)]. The scaling parameter A displays a peak for $x \approx 0.060$. The doping dependence of n and A is in agreement with the sharp increase in vortex dissipation for the $x = 0.060$ single crystal (see Fig. 5).

The fact that no doping dependence is found in m implies that the unconventional behavior in $\rho_{\rm ff}(H)$ is caused by the the same scattering mechanism of the quasiparticles around the vortex cores for samples belonging to the three doping regimes. On the other hand, n and A are most likely related to the magnetic degrees of freedom and their effect on the scattering of the flux vortices. Although further theoretical study is needed to understand more about this scaling behavior of the quasiparticle dissipation in the $Ba(Fe_{1-x}Co_x)_2As_2$ system, this I-V study strongly supports the change of the spin dynamics around the vortex core for the $x \approx 0.060$ samples.

D. Discussion

The motion of vortices in induced by the interaction between the circulating current around the vortex cores and the transport current. Specifically, the flux-flow is governed by the three forces: (i) Lorenz force $\vec{f}_L \propto \vec{j} \times \vec{B}$, where $\vec{j}$ is the transport current passing through the superconductor and $\vec{B}$ is the magnetic induction, (ii) pinning force $\vec{f}_{\rm pin}$, which is due to the interaction between pinning centers in the sample and flux vortices, and (iii) viscosity force $\vec{f}_v = -\eta\vec{v}_L$, where $\eta(H,T,x)$ is the viscosity coefficient characterizing the bulk superconducting properties of the material and v_L is the velocity of the flux vortices [25,26]. The pinning force depends on the interaction between flux lines and disorder potential, so that, when the transport current j exceeds some value $j_{\rm pin}$, the pinning force decreases with increasing vortex velocity. Thus, the only source of dissipation in the flux-flow regime (i.e., when $I \propto V$) is governed by the motion of the flux vortices since the interaction effects between the flux vortices and the pinning centers can be ignored. It follows that the flux-flow conductivity can be found from the following expression [25]:

$$\sigma_{\rm ff} = \frac{c^2}{\phi_0 B}\eta(H,T,x), \tag{2}$$

where $\phi_0 = hc/2e$ is a quantum of flux.

Generally speaking, the viscosity coefficient $\eta \simeq \phi_0 H_{c2}/\rho_n c^2$ is expected to be essentially independent of magnetic field and temperature, which is indeed the case for *conventional* single-band superconductors: flux-flow measurements routinely demonstrated that the flux-flow resistivity grows linearly with magnetic field. Interestingly, as it has been theoretically shown by Silaev and Vargunin [10], the linear B dependence of the flux-flow resistivity holds even in the case of multiband superconductors, although the resistive properties remain nonuniversal and depend on the system's specifics such as density of states for each band, retardation effects related to the relaxation of the superconducting order parameter, etc. [27,28]. In particular, the viscosity coefficient is shown to be given by $\eta = \pi\hbar\sum_k \nu_F^{(k)}(\alpha_k + \gamma_k)$, where $\nu_F^{(k)}$ is the density of states of the kth band and coefficients α_k and γ_k are determined by the superconducting order parameter $\Delta_k(r)$ and the single particle distribution function on the kth band. In other words, even in multiband superconductors η still remains independent of the magnetic field at least in the limit of low temperatures $T \ll T_c$, and small fields $H \ll H_{c2}$, where analytical calculations can be carried out.

Previous theoretical frameworks cannot be directly applied to the analysis of our data, since, for reasons discussed above, all the experimental data are taken at $T \sim T_c$. Furthermore, the fitting of our flux-flow resistivity data at temperatures $T \sim T_c$, summarized by Eq. (1), shows that the viscosity coefficient in the multiband $Ba(Fe_{1-x}Co_x)_2As_2$ superconducting alloys is strongly field dependent since $\rho_{\rm ff}$ does not increase linearly with H. Therefore, the T, H, and x dependence of η can be derived in the limit $h = H/H_{c2} \ll 1$ by using the Taylor expansion in powers of the parameter h in Eq. (1) and replacing $\sigma_{\rm ff}$ in Eq. (2) with the result from this Taylor expansion. It follows:

$$\frac{\eta(H,T,x)}{\eta(H_{c2},T,x)} \approx h[1 + a_1(T,x)h + a_2(T,x)h^2], \tag{3}$$

where $a_{1,2}$ are expansion coefficients that show strong dependence on the cobalt concentration x. In fact, both of these coefficients are $O(1)$ for $x \sim 0.060$, where the coexistence between the SDW and superconductivity has been observed.

Unfortunately, the microscopic origin of the effects which govern the values of the coefficients $a_{1,2}$ at this point remains obscure. We would like to note, however, that one would expect that the magnetic field itself affects the strength of magnetic fluctuations due to incipient SDW order and, as a result, causes the reduction in η. In this regard, it has been shown recently that the SDW order can emerge inside the vortex cores in the iron-based superconductors [29]. As a

consequence, one may speculate that the onset of the SDW order inside the vortex core affects the drag force and results in the magnetic field dependence of the drag coefficient. Indeed, both the superconducting order parameter and single-particle distribution function become dependent on the value of the SDW order parameter $\vec{M}(\vec{r})$ inside the vortex cores and, therefore, one may expect that the fluctuations of $\vec{M}$ will affect the relaxation of the superconducting order parameter, thus contributing to energy dissipation. Nevertheless, our data show that these effects appear to be very weak in regards to the flux-flow resistivity.

The presence of the weak anomalous increase of $\rho_{\rm ff}$ with decreasing H and T in the underdoped and overdoped regimes could indicate the emergence of SDW order inside the vortex cores. Interestingly, a similar effect has been studied in $CeCoIn_5$ [9], a completely different unconventional superconductor that belong to the 115 family of heavy fermion superconductors. In studying the magnetic fluctuations under the superconducting dome using I-V measurements to extract flux-flow dissipation, Hu and collaborators [9] have shown that the interplay between superconductivity and magnetism near and inside the vortex cores is also present in $CeCoIn_5$ in which partially unscreened local moments on Ce sites show tendency towards antiferromagnetic AFM order. They identified a scaling relationship from the $\rho_{\rm ff}(T,H,P)$ data and obtain an explicit equation for the AFM boundary inside the SC dome and an AFM QCP line that is accessed with two control parameters: H and P. However, they found a much weaker power-law dependence of $\rho_{\rm ff}(T,H)$ in $CeCoIn_5$, in contrast with the exponential dependence observed here in $Ba(Fe_{1-x}Co_x)_2As_2$ [see Eq. (1)]. This difference is most likely due to the nature of local moments in $CeCoIn_5$ compared to the itinerant magnetism in $Ba(Fe_{1-x}Co_x)_2As_2$. In addition, Park and collaborators have also studied the interaction between superconductivity and magnetism in the heavy fermion superconductor $CeRhIn_5$ and they have revealed the presence of a field-induced quantum phase transition (QPT) under the SC dome that separates coexisting SC and AFM phases from a pure unconventional SC phase [30].

The interplay between superconductivity and antiferromagnetism has also been studied in $La_{1.9}Sr_{0.1}CuO_4$ through neutron scattering, showing that its vortex state can be regarded as a mixture of a superconducting spin fluid and a core containing a nearly ordered SDW state that strengthen with increasing H [31,32]. In order to account for this result, Demler and co-workers proposed a model that assumes that the superconducting state is near a QPT to a state with microscopic coexistence of SC and magnetic orders [33]. They have shown that when H penetrates an unconventional superconductor in which the SC energy gap has nodes on the Fermi surface, field-induced quantized vortices have a magnetic ground state that suppresses superconductivity around the vortices. The suppression of the SC order enhances the competing SDW order even outside of the normal vortex cores, thus delocalizing magnetic correlations and creating microscopic coexistence of the SDW and SC orders. The repulsive coupling between SDW and SC orders can be tuned (by chemical substitution or pressure) to tip the balance between the two competing ground states, leading to QPTs among the pure SDW phase, the SDW and SC coexisting phases, and the pure SC phase.

IV. CONCLUSION

Current-voltage measurements were performed at temperatures close to T_{c0} on superconductive $Ba(Fe_{1-x}Co_x)_2As_2$ single crystals with doping levels covering underdoped, optimally doped, and overdoped regimes. Significantly enhanced flux-flow resistivity was observed at $x = 0.06$, possibly related to the existence of the boundary between the purely superconducting phase and the phase where superconductivity coexists with the SDW order. The universal scaling behavior of $\rho_{\rm ff}(H,T,x)$ observed in all doping levels implies that the upturn is governed by the dissipation in the bulk excitations. The changes in the scaling parameters m, n, and A over a wide doping range is in agreement with the fact that changes in the magnetic order around the vortex cores are related to changes in ground state of the system for Co concentrations $x \sim 0.060$. Thus, based on the consistency between the doping level dependence of the upturn in flux-flow resistivity and the phase diagram, we conclude that the abnormal enhancement in $\rho_{\rm ff}$ at low fields is most likely connected to the SDW order around the vortex cores. Our results imply that the viscosity coefficient has strong magnetic field and temperature dependence governed by the systems' proximity to a magnetic instability.

ACKNOWLEDGMENTS

We gratefully acknowledge invaluable help from Alan Baldwin in electronic and software techniques and Shuai Zhang for helpful discussions and an initial critical reading of the manuscript. This work was supported by the Notional Science Foundation Grants DMR 1505826 and DMR 1506547 at KSU. T.H. acknowledges the support of Notional Science Foundation of China (NSFC), Grant No. 11574338, and XDB04040300. H. X. acknowledges the support of NSFC, Grant No. U1530402.

[1] R. M. Fernandes, D. K. Pratt, W. Tian, J. Zarestky, A. Kreyssig, S. Nandi, M. G. Kim, A. Thaler, N. Ni, P. C. Canfield, R. J. McQueeney, J. Schmalian, and A. I. Goldman, Phys. Rev. B **81**, 140501 (2010).

[2] C. R. Rotundu and R. J. Birgeneau, Phys. Rev. B **84**, 092501 (2011).

[3] J.-H. Chu, J. G. Analytis, C. Kucharczyk, and I. R. Fisher, Phys. Rev. B **79**, 014506 (2009).

[4] F. Ning, K. Ahilan, T. Imai, A. S. Sefat, R. Jin, M. A. McGuire, B. C. Sales, and D. Mandrus, J. Phys. Soc. Jpn. **78**, 013711 (2009).

[5] R. M. Fernandes, S. Maiti, P. Wölfle, and A. V. Chubukov, Phys. Rev. Lett. **111**, 057001 (2013).

[6] S. Arsenijević, H. Hodovanets, R. Gaál, L. Forró, S. L. Bud'ko, and P. C. Canfield, Phys. Rev. B **87**, 224508 (2013).

[7] A. P. Dioguardi, J. Crocker, A. C. Shockley, C. H. Lin, K. R. Shirer, D. M. Nisson, M. M. Lawson, N. apRoberts-Warren, P. C. Canfield, S. L. Bud'ko, S. Ran, and N. J. Curro, Phys. Rev. Lett. **111**, 207201 (2013).
[8] M. G. Vavilov and A. V. Chubukov, Phys. Rev. B **84**, 214521 (2011).
[9] T. Hu, H. Xiao, T. A. Sayles, M. Dzero, M. B. Maple, and C. C. Almasan, Phys. Rev. Lett. **108**, 056401 (2012).
[10] M. Silaev and A. Vargunin, Phys. Rev. B **94**, 224506 (2016).
[11] N. Ni, M. E. Tillman, J.-Q. Yan, A. Kracher, S. T. Hannahs, S. L. Bud'ko, and P. C. Canfield, Phys. Rev. B **78**, 214515 (2008).
[12] J.-P. Reid, M. A. Tanatar, X. G. Luo, H. Shakeripour, N. Doiron-Leyraud, N. Ni, S. L. Bud'ko, P. C. Canfield, R. Prozorov, and L. Taillefer, Phys. Rev. B **82**, 064501 (2010).
[13] M. A. Tanatar, N. Ni, S. L. Budko, P. C. Canfield, and R. Prozorov, Supercond. Sci. Technol. **23**, 054002 (2010).
[14] Y. B. Kim, C. F. Hempstead, and A. R. Strnad, Phys. Rev. **139**, A1163 (1965).
[15] J. Bardeen and M. J. Stephen, Phys. Rev. **140**, A1197 (1965).
[16] N. B. Kopnin and A. V. Lopatin, Phys. Rev. B **51**, 15291 (1995).
[17] N. B. Kopnin and G. E. Volovik, Phys. Rev. Lett. **79**, 1377 (1997).
[18] S. Kambe, A. D. Huxley, P. Rodière, and J. Flouquet, Phys. Rev. Lett. **83**, 1842 (1999).
[19] S. Nair, O. Stockert, U. Witte, M. Nicklas, R. Schedler, K. Kiefer, J. D. Thompson, A. D. Bianchi, Z. Fisk, S. Wirth, and F. Steglich, Proc. Natl. Acad. Sci. USA **107**, 9537 (2010).
[20] D. K. Pratt, W. Tian, A. Kreyssig, J. L. Zarestky, S. Nandi, N. Ni, S. L. Bud'ko, P. C. Canfield, A. I. Goldman, and R. J. McQueeney, Phys. Rev. Lett. **103**, 087001 (2009).
[21] T. Okada, H. Takahashi, Y. Imai, K. Kitagawa, K. Matsubayashi, Y. Uwatoko, and A. Maeda, Phys. Rev. B **86**, 064516 (2012).
[22] T. Okada, H. Takahashi, Y. Imai, K. Kitagawa, K. Matsubayashi, Y. Uwatoko, and A. Maeda, Physica C: Superconductivity **494**, 109 (2013), proceedings of the 25th International Symposium on Superconductivity (ISS 2012) Advances in Superconductivity XXV.
[23] T. Okada, Y. Imai, H. Takahashi, M. Nakajima, A. Iyo, H. Eisaki, and A. Maeda, Physica C **504**, 24 (2014), proceedings of the 26th International Symposium on Superconductivity .
[24] T. Okada, F. Nabeshima, H. Takahashi, Y. Imai, and A. Maeda, Phys. Rev. B **91**, 054510 (2015).
[25] A. R. Strnad, C. F. Hempstead, and Y. B. Kim, Phys. Rev. Lett. **13**, 794 (1964).
[26] A. I. Larkin and Y. N. Ovchinnikov, *Nonequilibrium Superconductivity* (North-Holland, Amsterdam, 1986), Vol. 12, p. 493.
[27] M. Tinkham, Phys. Rev. Lett. **13**, 804 (1964).
[28] L. P. Gor'kov and N. B. Kopnin, Sov. Phys. JETP **33**, 1251 (1971).
[29] V. Mishra and A. E. Koshelev, Phys. Rev. B **92**, 064511 (2015).
[30] T. Park, F. Ronning, H. Q. Yuan, M. B. Salamon, R. Movshovich, J. L. Sarrao, and J. D. Thompson, Nature (London) **440**, 65 (2006).
[31] B. Lake, G. Aeppli, K. N. Clausen, D. F. McMorrow, K. Lefmann, N. E. Hussey, N. Mangkorntong, M. Nohara, H. Takagi, T. E. Mason, and A. Schroeder, Science **291**, 1759 (2001).
[32] B. Lake, H. M. Ronnow, N. B. Christensen, G. Aeppli, K. Lefmann, D. F. McMorrow, P. Vorderwisch, P. Smeibidl, N. Mangkorntong, T. Sasagawa, M. Nohara, H. Takagi, and T. E. Mason, Nature (London) **415**, 299 (2002).
[33] Y. Zhang, E. Demler, and S. Sachdev, Phys. Rev. B **66**, 094501 (2002).